Silver Nanoplates/Graphene Oxide Nanocomposite for the Detection of Hydrogen Peroxide

Johanna Pilicita-Carua,[a] Gottfried Suppan,[a] Karla Vizuete,[b] Alexis Debut,[b] and Sarah Briceño [a*]

[a] Yachay Tech University, School of Physical Sciences and Nanotechnology, 100119 Urcuquí, Ecuador.
[b] Centro de Nanociencia y Nanotecnología, Universidad de las Fuerzas Armadas ESPE, Sangolqui, Ecuador

*Corresponding authors E-mail: pilicitajohanna@gmail.com and sarahbriara@gmail.com

ABSTRACT

Optimizing the electrochemical properties of carbon-based nanocomposites is a fundamental challenge for sensor applications. In this work, the optimization of the electrochemical properties of silver nanocomposites on graphene oxide was studied for the fabrication of a non-enzymatic hydrogen peroxide (H_2O_2) sensor. To do so, we transform silver nanoparticles (AgNP) into silver nanoplates (AgNC) and anchor them to graphene oxide (GO) via the photochemical reduction method at 540 nm irradiation wavelength for its deposition on the surface of graphite electrodes (GE) and detect low concentrations of H_2O_2. We performed a physicochemical characterization of the resulting nanocomposite using a combination of UV-Vis spectroscopy, scanning electron microscopy (SEM), transmission electron microscopy (TEM), and Raman spectroscopy, to then, analyze the electrochemical properties of GE modified with silver nanocomposites by cyclic voltammetry (CV). Our results reveal an improvement of the sensitivity from $309\ \mu A\,mM^{-1}\,cm^{-2}$ to $444\ \mu A\,mM^{-1}\,cm^{-2}$ and limits of detection (LOD) and limits of quantification (LOQ) from 0.68 mM and 2.29 mM to 0.28 mM and 0.96 mM using $AgNP/GO-GE$ and $AgNC/GO-GE$ nanocomposites electrodes, respectively. The enhancement of the electrochemical properties reveals a synergistic effect between the planar shape of the AgNC and the oxygen functional groups over the GO surface. In so doing, we have demonstrated the utility of a low-cost photoreduction method to optimize the structural properties of AgNC/GO and, in this way, enhance the electrochemical properties of the modified electrode for H_2O_2 sensing. These results should greatly interest a wide range of biomedical applications and medical devices.

Keywords: Nanotechnology; silver nanocomposites; modified electrodes; electrochemical sensing, electrochemical properties.

Nanocomposito de Nanoplacas de Plata/ Óxido de Grafeno para la Detección de Peróxido de Hidrogeno

RESUMEN

La optimización de las propiedades electroquímicas de nanocompuestos a base de carbono es un desafío fundamental para las aplicaciones de sensores. En este trabajo, estudiamos la optimización de las propiedades electroquímicas de nanocompositos de plata sobre óxido de grafeno para fabricar un sensor no enzimático de H_2O_2. Para hacerlo, transformamos nanopartículas de plata (AgNP) en nanoplacas de plata (AgNC) y las soportamos sobre GO utilizando el método de reducción fotoquímica a una longitud de onda de irradiación de 540 nm, para ser depositados en la superficie de electrodos de grafito (GE) y detectar bajas concentraciones de H_2O_2. Realizamos una caracterización fisicoquímica del nanocompuesto utilizando una combinación de espectroscopia UV-Vis, microscopia electrónica de barrido (SEM), microscopia electrónica de transmisión (TEM) y espectroscopia Raman, para después, analizar las propiedades electroquímicas de los GE modificados con nanocompositos metálicos mediante voltametría cíclica (CV). Los resultados revelan una mejora de la sensibilidad de 309 $\mu A\,mM^{-1}\,cm^{-2}$ a 444 $\mu A\,mM^{-1}\,cm^{-2}$ y límites de detección (LOD) y límites de cuantificación (LOQ) de 0,68 mM y 2,29 mM a 0,28 mM y 0,96 mM usando los electrodos modificados con $AgNP/GO-GE$ y $AgNC/GO-GE$ respectivamente. Esta mejora muestra un efecto sinérgico entre la forma plana de las nanoplacas y los grupos funcionales en la superficie del GO, demostrando la utilidad de la fotoreducción para optimizar las propiedades estructurales de los nanocompositos de plata y, así, mejorar sus propiedades electroquímicas para detectar H_2O_2. Estos resultados son de interés para una amplia gama de aplicaciones y dispositivos biomédicos.

Palabras claves: Nanotecnología; nanocompositos de plata; electrodos modificados; detección electroquímica; propiedades electroquímicas.

INTRODUCTION

Nanocomposites based on metallic nanoparticles on graphene oxide are of particular interest due to their extraordinary electrochemical, optical, catalytic, and antibacterial properties [1]. These properties depend on the nature of the nanomaterials, the shape, size, and distribution of the nanoparticles over GO [2]. In this sense, the presence of the oxygen functionalities at the GO surface provides reactive sites for the nucleation and growth of metallic nanoparticles [2]. Graphene oxide (GO) has become one of the most studied two-dimensional (2D) materials due to its exceptional properties, especially electrocatalytic, high conductivity, and surface area [3]. GO is a single atomic layer thick sheet of hexagonally arranged sp2 carbon atoms, with many free electrons, which can be used to reduce metallic ions to produce the hybrid material consisting of metallic nanoparticles on the 2D fabric of GO [3]. The deposition and growth of metallic nanoparticles on GO could enhance the electrochemical properties of carbon-based electrodes, which is an important feature to be applied in the sensing field [4]. The development of low-cost and high-sensitivity electrode materials and techniques for accurate, fast, and reliable detection of hydrogen peroxide (H_2O_2) is of great importance [5]. (H_2O_2) is considered an essential component used in many fields of industry and is widely used in clinical, biomedical, environmental, pharmaceutical, and many other fields [6]. There are several reports where spherical nanoparticles are used for the electrochemical detection [5][6][7]. However, few promote using flat nanoparticles such as nanoprism or nanocubic shapes with enhanced surface properties to improve the recognition signal in the detection process. Yang et al [8] report the application of modifying glassy carbon electrodes with silver nanoparticles on GO for electrochemical sensing of H_2O_2 showing promising results. Saade and Araújo [9] report the photochemical method for synthesizing silver nanoprisms. Based on their results, was recently reported the growth of silver nanoprism on graphene oxide using the photochemical method.

In this work , we optimize the surface properties of silver nanocomposites suspended on GO, using the photochemical reduction method at 540nm excitation wavelength for the electrochemical detection of H_2O_2 through electrochemical methods using graphite electrodes modified with silver nanoplates on GO producing an enhanced signal which can be easily detected. Our results reveal the photoconversion of the silver nanoparticles to obtain nanoplates on GO. In addition, the electrochemical characterization determined the potential of the silver nanocomposites modified electrodes in the detection of H_2O_2 concentrations between 0.4 mM to 3 mM. The advantage of this work is the fabrication of low-cost silver graphene-based electrodes with enhanced detection signals for low concentrations of H_2O_2.

MATERIALS AND METHODS

1.1. Chemicals

Silver nitrate $AgNO_3$ 99%, sodium borohydride $NaBH_4$ 98%, and polyvinyl alcohol (PVA), average $Mw\ 85,000 - 124,000\ 87 - 89\%$ hydrolyzed were purchased from Sigma Aldrich. Trisodium citrate $Na_3C_6H_5O_7$ 99% and hydrogen peroxide H_2O_2 30% were purchased from Lobachemie. Ammonium hydroxide NH_4OH 1%, sodium chloride NaCl 99%, and sulfuric acid H_2SO_4 98% were purchased at a local supplier. Graphene oxide powder was purchased from Abalonyx Innovative materials. Potassium ferricyanide $K_3[Fe(CN)_6]$ 99%, and phosphate buffer 98% at a pH of 7 were purchased from

Fisher Chemical. All chemicals were of analytical grade and were used as received without further purification.

1.2. Synthesis of AgNP/GO and AgNC/GO

nanocomposites

Quasi-spherical silver nanoparticles were synthesized in 28,4 mL of demineralized water under vigorous stirring at room temperature by adding 150 μL of 50 mM $AgNO_3$ and 400 μL of 75mM $Na_3C_6H_5O_7$ as the silver precursor and the capping agent, respectively. After 3 min, 4 μL of 100mM $NaBH_4$ were added to reduce ionic to metallic silver, forming silver nanoparticles in a light yellow solution. Then, 60 μL of 30% H_2O_2 were added as the etching agent to promote the formation of planar structures by the dislocation in the atomic planes of nanoparticles due to their low stacking-fault energy [10], leading to a colorless solution. Finally, 250 μL of 100 mM $NaBH_4$ were rapidly injected to obtain silver nanoparticles (AgNP) in a reddish-yellow solution. Simultaneously a homogeneously dispersed solution of graphene oxide was prepared by adding 10 μL of PVA 1 wt% to 10 mL of 0.1 wt% of graphene oxide and putting it under sonication for 2h at room temperature. Silver-graphene oxide nanocomposite (AgNP/GO) was formed by mixing down agitation at room temperature 50 μL of 1% NH_4OH, with 976 μL of GO solution, and 30 mL of silver nanoparticles previously prepared.

1.3. Photoreduction process

The photoreduction process was performed using a simple and low- cost, high-power light chamber fabricated following the methodology proposed by Saade & Araújo [9] .This setup consists of a PVC tube of 17 cm in longitude and 11.5 cm in diameter. As a light source, we used high-power LEDs of 5 watts. Six LEDs of 540 nm excitation wavelength were connected in series and placed at the bottom of the PVC tube to fabricate the chamber. The LEDs were equidistantly placed inside the chamber to

ensure the energy distribution toward the sample, forming a ring. Aluminum foil was used at the top of the PVC tube to avoid any external light contamination to close the chamber. Finally, the previously prepared AgNP/GO nanocomposite were put in a vessel of 15 mL inside the PVC light chamber and irradiated with 540nm excitation wavelength for 16 h at room temperature, as illustrated below in Figure 1. After the photochemical reduction process at 540nm, the color of the sample changed from reddish-yellow to blue as the first qualitative optic evidence of the transformation of the silver nanoparticles (AgNP/GO) to silver nanoplates (AgNC/GO) nancomposites.
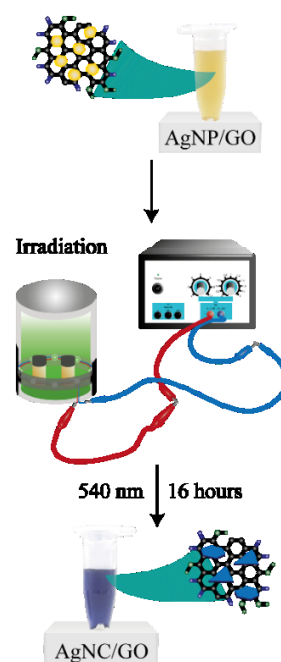

Figure 1. Photoreduction process of silver nanoparticles on graphene oxide (AgNP/GO) to obtain silver nanoplates on graphene oxide (AgNC/GO)

1.4. Characterization

The optical properties were measured using a Genova Nano Jenway UV-Vis spectrophotometer. SEM micrographs were acquired by a Scanning Electron Microscope PHENOM PRO X from AMPTEK with a backscattered electron detector (BSD). TEM micrographs

were obtained at 80 kV using an FEI-Tecnai G20 Spirit Twin microscope equipped with an Eagle 4k HR camera. Raman measurements were acquired using a HORIBA LabRAM HR Evolution spectrometer at 532 nm. Cyclic voltammetry analyses were recorded with a Stat300 potentiostat driven by DropView 8400 software.

RESULTS AND DISCUSSION
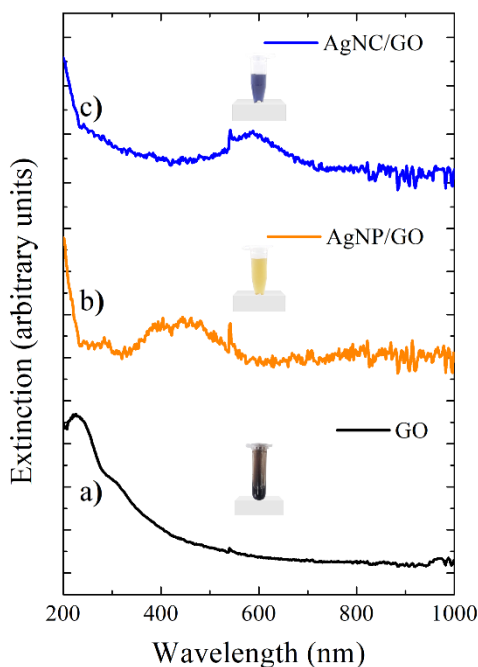
2.1. UV-Vis spectroscopy

Figure 2. UV-Vis extinction spectra of a) graphene oxide (black), b) $AgNP/GO$ before being irradiated (orange), and c) $AgNC/GO$ after the photoreduction process (blue).

$Figure\ 2\ (a)$ shows the extinction spectra of GO (black). In this spectra, the first absorption at $226\ nm$ corresponds to the $\pi \rightarrow \pi^*$ transition of $C - C$, and the second peak as a shoulder is centered at $301\ nm$ corresponds to $n \rightarrow \pi *$ transitions of $C = O$ [11]. In $Figure\ 2\ (b)$ the spectra of the $AgNP/GO$ nanocomposite, before being irradiated, exhibit two main absorption bands. The first surface plasmon resonance (SPR) is observed at $284\ nm$, and it is related to $n \rightarrow \pi *$ transitions of $C = O$ bonds in GO. This

absorption confirms the interaction between silver nanoparticles and graphene oxide and exhibits a blue shift suggesting a reduction of graphene oxide during the photoreduction process [12].   Then, the strongest plasmonic band is centered at $437\ nm$ due to the formation of spherical-shaped $AgNP/GO$ [13]. After the photochemical reduction process, in $Figure\ 2\ (c)$, the spectra of $AgNC/GO$ nanocomposite show the strongest plasmonic band at $586\ nm$ suggesting the transformation of silver nanoparticles to form nanoplates $AgNC - GO$ nanocomposite [14], as we will confirm by SEM and TEM.
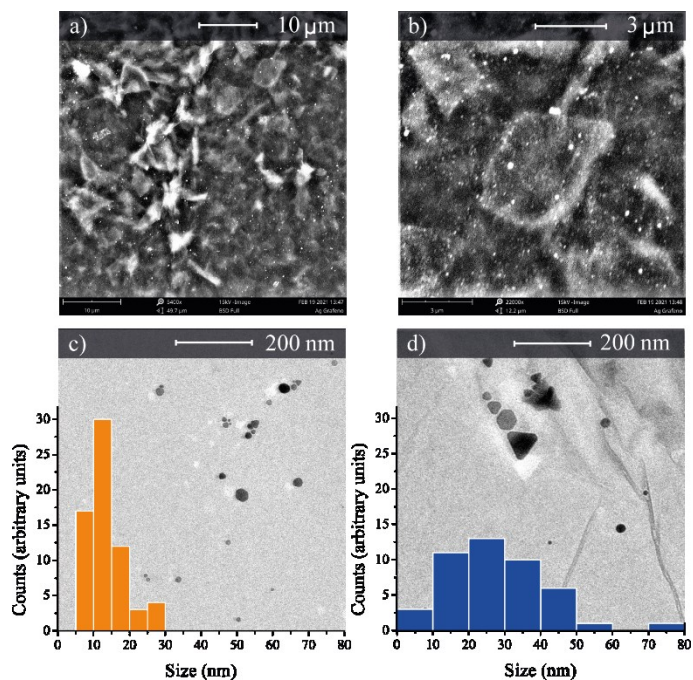
2.2. Microscopy techniques

Figure 3. Microscopy characterization. a) and b) SEM micrographs of $AgNC/GO$ nanocomposite, and TEM images of: c) $AgNP/GO$ nanocomposite before being irradiated and d) $AgNC/GO$ nanocomposite after the photoreduction process. Insets: Average particle size histograms from TEM.

$Figure\ 3\ a)$ and $b)$ presents the scanning electron micrographs of $AgNC/GO$ nanocomposite after the

photoreduction process at $540\ nm$. In these micrographs, we identify the presence of GO sheets with an average size of $4\ \pm\ 1\ \mu m$ and a homogeneous distribution of the silver nanoparticles on GO. As well, transmission electron micrographs in $Figure\ 3\ c)$ and $d)$ demonstrate that silver nanoparticles were transformed after the photoreduction process, from quasi-spherical $AgNP/GO$ of $12 \pm 3\ nm$ to a bimodal size distribution of planar nanostructures ($AgNC/GO$) of $25 \pm 5\ nm$ and $75 \pm 5\ nm$ after the photoreduction process at $540\ nm$. The formation of $AgNC/GO$ could be explained by the effect of TSC that allows the growth along the lateral direction and the blocking growth along its vertical direction [10]. During the nucleation process, silver ions were reduced to metallic silver to form Ag nanoparticles, TSC were used as a stabilizer during the synthesis to avoid agglomeration. When the nanocomposite was exposed to light irradiation at $540\ nm$, the excess of ions generated around the silver nanoparticles was reduced. At the same time, TSC allowed the formation of planar structures including mainly nanoplates and hexagons [15].
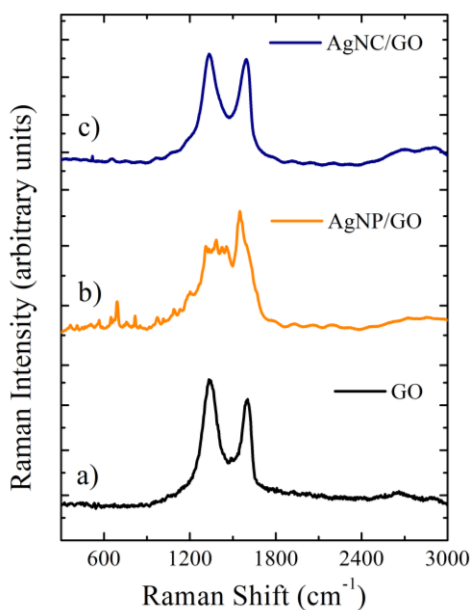
2.3. Raman spectroscopy

Figure 4. Raman spectra of a) GO, b) $AgNP/GO$ before being irradiated, and c) $AgNC/GO$ after the photoreduction process.

Raman spectra of the nanocomposites before and after the photoreduction process are shown in $Figure\ 4$. In these spectra, the first peak was observed at $1342\ cm^{-1}$ assigned to the D band related to out-of-plane vibrations and attributed to the defects in the sp^2-hybridized carbon, and the second peak at $1607 cm^{-1}$ is associated to the G band that corresponds to the first-order scattering of the E_{2g} mode of graphene [16][17]. For the $AgNP/GO$ and $AgNC/GO$ spectra, the D and G intensities are enhanced compared to the GO spectra. This effect could be explained by the growth of silver nanoparticles on the surface GO causing the increasing band intensities due to the high electromagnetic field of the silver nanoparticles, producing a Surface-Enhanced Raman Scattering effect [11]. Also, a broad 2D band at $2798\ cm^{-1}$ is observed in the Raman spectra of $AgNC/GO$ associated with the thickness of GO, confirming the presence of few-layer graphene oxide [18]. Additionally, a band at $691\ cm^{-1}$ for $AgNP/GO$ and $516\ cm^{-1}$ for $AgNC/GO$ appears, corresponding to the $Ag-O$ vibration on GO [19]. Figure 4 reports the intensity ratios (I_D/I_G), showing that the intensity ratio is higher for GO compared to $AgNP/GO$ and $AgNC/GO$ nanocomposites. Although incorporating Ag nanoparticles on GO means including more defects in its structure, silver nanoparticles may fulfill the isolated bonds from GO to oscillate at a coherent frequency, generating order vibrations and reducing the ratio of defects. Raman spectra evidence the interaction between $AgNP$, $AgNC$ and GO.

2.4. Electrochemical Analysis

2.4.1. Cyclic Voltammetry

Cyclic voltammetry was used to compare the electrochemical behavior of $AgNP/GO$ and $AgNC/GO$

nanocomposites deposited on the surface of a graphite electrode (GE). *Figure* 5 *a*) shows the electrochemical window for the bare GE, as well as for $AgNP/GO-GE$ and $AgNC/GO-GE$ in $1\,wt\%\,NaCl$. As shown in *Figure* 5, the window for GE is slightly smaller than for $AgNP/GO-GE$ and $AgNC/GO-GE$. $AgNP/GO-GE$ and $AgNC/GO-GE$ show similar voltammograms, including oxidation peaks at $-0.1\,V$. Furthermore, the position of the oxidation peak at $-0.11\,V$ for $AgNP/GO-GE$ indicates higher stability for this electrode compared to $AgNC/GO-GE$ at $-0.1\,V$ [20].
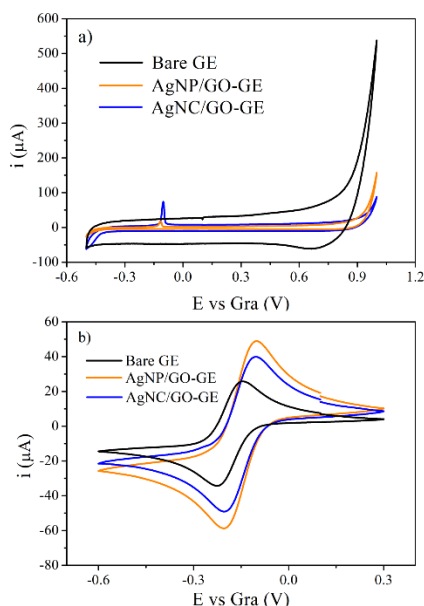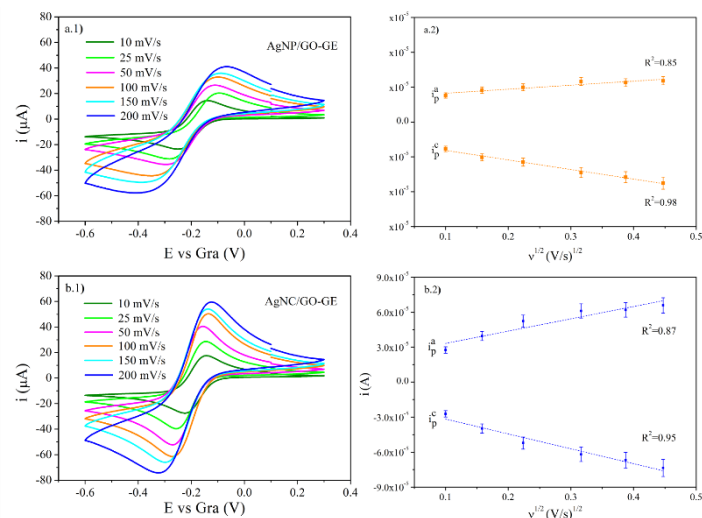

or $AgNC/GO-GE$, revealing that the modified electrodes enhance the redox current response due to the conductive properties of the nanocomposites on the surface of the electrode, facilitating the electron transfer process [6][17].

Figure 6. Cyclic voltammograms using $2.5\,mmol\,K_3[Fe(CN)_6]$ at different scan rates: 10; 25; 50; 100; 150; 200 $\frac{mV}{s}$ and Randles-Sevcik plots of peak current (i) against the square root of scan rate (v) for anodic and cathodic peaks at ($a.1$ and $a.2$) $AgNP/GO-GE$, and ($b.1$ and $b.2$) $AgNC/GO-GE$.

Figure 5. Cyclic voltammograms of GO, $AgNP/GO-GE$, and $AgNC/GO-GE$ in: a) $NaCl$ ($1wt$ %) at a scan rate of $100\,mV$, and b) $2.5\,mM\,K_3[Fe(CN)_6]$ in $0.1\,M\,KCl$ at a scan rate of $50\,\frac{mV}{s}$

The redox behavior of $2.5\,mmol\,K_3[Fe(CN)_6]$ in $0.1\,mol\,KCl$ at bare GE, $AgNP/GO-GE$ and $AgNC/GO-GE$, is observed in *Figure* 5 *b*). The redox reactions of $Fe(CN)_6^{3/4}$ at all electrodes show high reversible electrochemical behavior with a peak separation of about $80\,mV$ with an anodic-cathodic peak ratio of 1. It can also be observed that the magnitude of the redox current at the bare GE is lower than for $AgNP/GO-GE$

Cyclic voltammograms using $2.5\,mmol\,K_3[Fe(CN)_6]$ in $0.1\,mol$ of phosphate buffer at a varying scan rate were recorded to study the diffusion behavior of the redox species using $AgNP/GO-GE$ and $AgNC/GO-GE$ samples, as shown in *Figures* 6 ($a.1$ and $b.1$), respectively. The voltammograms measured for both samples reveal that the oxidation and reduction peak potentials (E_p^a and E_p^c, respectively) drift apart with the increase of the scan rate, leading to an increase of the potential peak separation, ΔE_p. Additionally, the magnitude of the redox peak current indicates a direct proportionality with the scan rate. In general, the voltammograms suggest a reversible behavior. A comparison between the voltammograms for $AgNP/$

$GO - GE$ and $AgNC/GO - GE$ in *Figures* 6 (*a*. 1 and *b*. 1) indicates a dependence of the current signal on the sizes and shapes of the nanostructures, as the irradiated nanostructure-based electrodes magnify the signal intensities. Randles-Sevcik analysis was performed for $AgNP/GO - GE$ and $AgNC/GO - GE$ to obtain the graphs of i against $v^{1/2}$ using the *equation* 1. The analysis was made for the anodic and cathodic peaks as shown in *Figures* 6 (*a*. 1 and *b*. 1), respectively, to obtain *Figures* 6 (*a*. 2 and *b*. 2) and extract the values of the diffusion coefficients D. Randles-Sevcik analysis was performed for $AgNP/GO - GE$ and $AgNC/GO - GE$.

$$i_p = 0.4463c \frac{(nF)^{\frac{3}{2}}}{(RT)^{\frac{1}{2}}} A (D_i v)^{1/2} \qquad (1)$$

Where i_p is the anodic or cathodic peak, A is the electroactive area, c is the concentration of the analyte, n is the number of transferred electrons in the redox reaction, F is the Faraday's constant, R is the gas constant, T is the temperature, D_i is the anodic or cathodic diffusion coefficient, and v is the scan rate. The linear tendency observed in the plots of redox peak current in *Figure* 6 indicates a diffusion-controlled mechanism of the mass transfer process [21] [22].

Finally, the calculated diffusion coefficients for the oxidized (D^a) and reduced (D^c) species are $2.38 \times 10^{-8} cm^2 s^{-1}$ and $1.34 \times 10^{-7} cm^2 s^{-1}$ for $AgNP/GO - GE$, while for $AgNC/GO - GE$ are $2.20 \times 10^{-7} cm^2 s^{-1}$ and $3.21 \times 10^{-7} cm^2 s^{-1}$ respectively, as shown in Table 1, indicating no specific influence of the electrode surface composition on the sizes and shapes of the nanoparticles on the diffusion process [23][24][25].

Table 1. Diffusion coefficients of $AgNP/GO - GE$, and $AgNC/GO - GE$ at anodic and cathodic peaks.

Electrode	D^a ($cm^2 s^{-1}$)	R^2
AgNP/GO − GE	2.38×10^{-8}	0.85
AgNC/GO − GE	2.20×10^{-7}	0.98
Electrode	D^c ($cm^2 s^{-1}$)	R^2
AgNP/GO − GE	1.34×10^{-7}	0.87
AgNC/GO − GE	3.21×10^{-7}	0.95

The reversibility of the electrochemical reaction of $Fe(CN)_6^{3/4}$ on $AgNP/GO - GE$ and $AgNC/GO - GE$ was studied by determination of the heterogeneous rate constant, k^0, based on the works by Nicholson, which relate dimensionless kinetic parameter ψ to the heterogeneous rate constant k^0 according to the following equation [25].

$$\psi = k^0 \left(\frac{\pi D_i nvF}{RT} \right)^{-1/2} \qquad (2)$$

Furthermore, ψ can be related to the experimentally accessible redox peak potential separation, ΔE_P, as shown by Lavegnini *et al* by equation:

$$\psi = 2.18 \left(\frac{\alpha}{\pi} \right)^{1/2} \exp \left(\frac{\alpha^2 F}{RT} n \Delta E_p \right) \qquad (3)$$

where α is the charge transfer coefficient and all other symbols maintain their previously defined meaning. Finally, α can be determined from the cyclic voltammograms through equation 4.

$$\alpha = \frac{1.875 \, RT}{nF|E_p - E_{p/2}|} \qquad (4)$$

Where E_p is the peak potential, $E_{p/2}$ the half- peak potential and the other symbols have already being defined. The calculated heterogeneous standard rate constants at oxidized and reduced species for $AgNP/GO - GE$ are $9.46 \times 10^{-5} cm \, s^{-1}$ and $2.25 \times 10^{-4} cm \, s^{-1}$ respectively, then for $AgNC/GO - GE$ are $6.27 \times 10^{-4} cm \, s^{-1}$ and $7.58 \times 10^{-4} \, cm \, s^{-1}$, as seen in Table 2, mainly in agreement with the literature [25], additionally, the biggest values of k^0 were calculated for $AgNC/GO - GE$ indicating the faster speed of the electron transfer between the electrode surface and the electroactive redox species [26][27].

Table 2. Standard rate constant (k^0) of $AgNP/GO - GE$, and $AgNC/GO - GE$ at anodic and cathodic peaks.

Anodic

Electrode	k^0 (cm s^{-1})	$\pm$Error (cm s^{-1})
AgNP/GO − GE	9.46×10^{-5}	1.45×10^{-5}
AgNC/GO − GE	6.27×10^{-4}	7.05×10^{-5}
Cathodic		
AgNP/GO − GE	2.25×10^{-4}	3.45×10^{-5}
AgNC/GO − GE	7.58×10^{-4}	8.51×10^{-5}

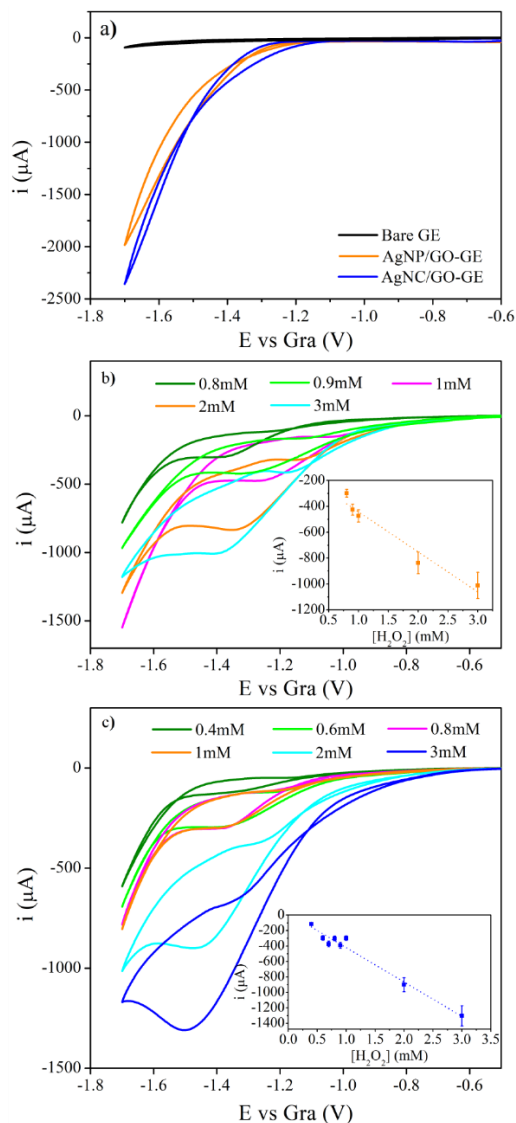### 2.4.2. *Electrocatalytic reduction of H_2O_2*

Figure 7. Cyclic voltammograms for different concentrations of H_2O_2 in $0.1\,M$ phosphate buffer recorded at a scan rate of $50\ mVs^{-1}$ at room temperature: a) Bare GE, and modified Ag-nanocomposite electrodes without H_2O_2. b) $AgNP/GO − GE$ in the presence of

H_2O_2 ($0.8\,mM$ to $3\,mM$). c) $AgNC/GO − GE$ in the presence of H_2O_2 in concentrations between $0.4\,mM$ to $3\,mM$. Insets: Peak current (i) vs concentration of $[H_2O_2]$.

The electrocatalytic activity of $AgNP/GO − GE$ and $AgNC/GO − GE$ for the reduction of H_2O_2 in different concentrations were analyzed in $0.1\,M$ phosphate buffer at a pH of 7.2, as a potential material to fabricate sensors with enhanced electrocatalytic properties. Figure 7 (a) shows the absence of non-analyte signal related to redox signals when any H_2O_2 concentration is not detected in the buffer solution. *Figure* 7 (*b*) shows the electrochemical reduction of H_2O_2 at $AgNP/GO − GE$, which is identified as a cathodic current starting at around $-0.8\,V\ vs\ Gra$ and characteristic cathodic current peaks between $-1.2\,V$ and $-1.6\,V$. The lowest visible change in the CV was recorded at a H_2O_2 concentration of $0.8\,mM$ and the highest lineal response (inset in *Figure* 7 (*b*)) was recorded at $3\,mM$. *Figures* 7 (*c*) shows that the signal response at $AgNC/GO − GE$ reaches smaller H_2O_2 concentrations between $0.4\,mM$ and $3\,mM$ compared to $AgNP/GO − GE$, which implies a more facilitated electron transfer that is attributed to the sizes and shapes of the silver nanostructures [4]. Therefore, the planar nanostructures that predominate in $AgNC/GO − GE$ samples generate a greater range of sensitivity, which can be attributed to the effect of the near field enhancement of the nanoplates compared to quasi-spherical shapes in $AgNP/GO$ nanocomposite. The highest linear response of the nanocomposite could be explained by the electrocatalytic activity generated on the surface of the electrode by the synergistic effect of the silver nanoplates on GO and the direct interaction of the nanoplates in the electrocatalytic reduction process [28][6].

Sensitivity, limits of detection (LOD) and quantification (LOQ) were calculated [29] from the lineal responses shown in the insets of *Figures* 7 (*b* and *c*) for

$AgNP/GO - GE$ and $AgNC/GO - GE$, respectively. The performance metrics are detailed in *Table* 2, showing a sensitivity of $309.55 \ \mu A \ mM^{-1} \ cm^{-2}$ for $AgNP/GO - GE$ and $444.51 \ \mu A \ mM^{-1} \ cm^{-2}$ for $AgNC/GO - GE$ which indicates an improvement of around 44 %. Also the LOD and LOQ increase from $0,68 \ mM$ and $2,29 \ mM$ respectively for $AgNP/GO - GE$ to $0,28 \ mM$ and $0,96 \ mM$ respectively for $AgNC/GO - GE$, thus increasing sensing capabilities by a factor greater than two. This suggests that the introduction of planar nanostructures improve the electrochemical properties of ultrasensitive sensor materials [6] and in this case, outperforms spherically shaped nanoparticles. Several performance metrics for similar Ag-based electrochemical sensors reported in the literature indicate smaller values of sensitivity, for example, Viswanathan, P *et al*. reports a sensitivity of $34 \ \mu A \ mM^{-1}$ for an electrode based on silver nanoparticles synthetized in the presence of polymers [30], also Noor, A. *et al*. indicates a sensitivity of $0.12 \ \mu A \ mM^{-1}$ at a modified glassy carbon electrode with silver nanocomposites [6], this comparison reveals promising and favorable results for the $AgNP/GO - GE$ and $AgNC/GO - GE$ synthesized on this work.

Table 3. Metrics performance of $AgNP/GO - GE$, and $AgNC/GO - GE$ and a comparison with sensors based on silver nanoparticles cited in the literature.

Electrode	Linearity	Sensitivity
AgNP/GO − GE	0.8-3.0 mM	309.55 $\mu A \ mM^{-1} \ cm^{-2}$
AgNC/GO − GE	0.4-3.0 mM	444.51 $\mu A \ mM^{-1} \ cm^{-2}$
AgNPs [30]	0.005-0.4 mM	0.034 $mA \ mM^{-1} \ cm^{-2}$
AgNPs@GC [6]	0.005-4.0 mM	0.16 $mA \ mM^{-1} \ cm^{-2}$
Electrode	**LOD**	**LOQ**
AgNP/GO − GE	0.68 mM	2.29 mM
AgNC/GO − GE	0.28 mM	0.96 mM
AgNPs [30]	5.0 μM	-
AgNPs@GC [6]	1.7 μM	-
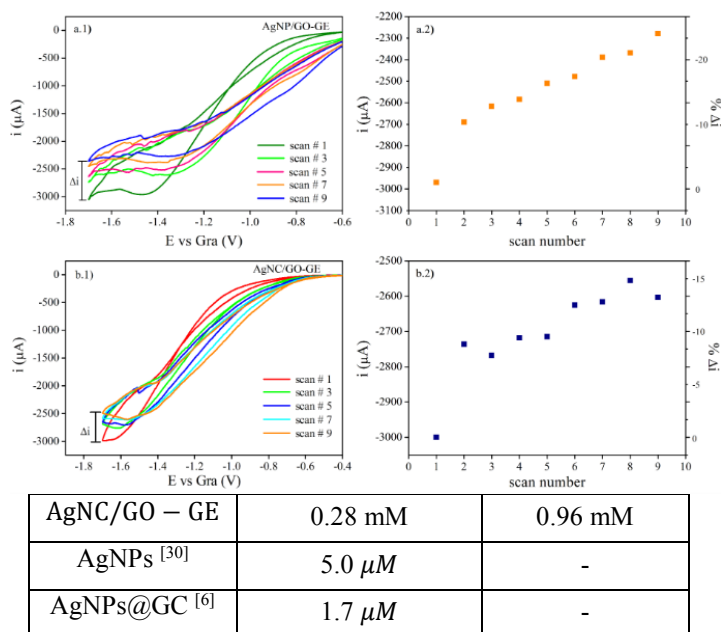
2.4.3. Stability of the nanocomposite based electrodes

Figure 8. Stability test performed by recording several cyclic voltammograms with a scan rate of $50 \ mV \ s^{-1}$, and percentual decay of the electrochemical signal as a function of the scan number at $6 mM \ H_2O_2$ in $0.1 \ M$ phosphate buffer at: $(a.1$ and $a.2)$ $AgNP/GO - GE$, and $(b.1$ and $b.2)$ $AgNC/GO - GE$. Only selected scans are chosen for visibility.

To study the oxidation stability of the silver nanoparticles deposited on the surface of graphite electrodes, nine consecutive cyclic voltammograms were recorded between $-1.7 \ V$ and $0 \ V \ vs \ Gra$ at a scan rate of $50 \ mV \ s^{-1}$ in an oxidizing environment. The measurements revealed nanostructure-dependent changes

in the signal response, expressed as a percentage decrease compared to the initial signal (%Δi), as illustrated in Figure 8. *Figure* 8 (*a*. 1) shows the stability test using $6\ mM$ hydrogen peroxide in $0.1\ M$ phosphate buffer at $AgNP/GO - GE$ indicating a current difference between the first (1) and the last scan (9) of %$\Delta i = 690\ \mu A$, and the detected current at the last scan reaches a value around $-2278\ \mu A$. The percentual decay in *Figure* 8 (*a*. 2) shows a current signal decreasing following a linear tendency until reaching a decay of $-23\ \%$. In *Figure* 8 (*b*. 1) the stability test of $AgNC/GO - GE$ reveals the %$\Delta i = 396\ \mu A$, and detecting the last scan (9) around $-2604\ \mu A$. *Figure* 8 (*b*. 2) also shows the decrease of the signal following a linear tendency, but in this case, until reaching

a decay of -15%. The smallest %Δi value is observed for $AgNC/GO - GE$ samples, which demonstrates that the stability of the $AgNC/GO$ composite electrode is higher than $AgNP/GO$ and depends on the shapes and sizes of the nanoparticles on the surface of the electrodes. Although, to the author's knowledge, the shape dependence of the resistance of silver nanoparticles towards oxidation has not yet being reported, higher oxidation rates for smaller spherical NPs than of their larger counterparts have being reported [31]. As can be seen in *Figure* 3*d*, the micrograph of the $AgNC -$based sample shows rather larger particle sizes compared to the $AgNP -$based one (*Fig.* 3*c*), therefore serving as a possible explanation besides the difference in shape between the sample.

CONCLUSIONS

In this work, we demonstrated the use of silver nanoplates on GO as electrocatalyst support for the nonenzymatic sensing of H_2O_2. The photoreduction process strongly strengthens the silver nanoparticles transformation, enabling the synthesis of well-dispersed nanoplates supported on GO. The electrode kinetics of $AgNP/GO -$

GE and $AgNC/GO - GE$ extracted by the analysis of diffusion coefficients and the standard rate constant exhibit an electrochemical response comparable and superior to more sophisticated and expensive electrodes, which could be attributed to the synergetic effects between the nanoplates on GO, in which the planar shape of the nanoparticles plays a significant role in promoting the H_2O_2 detection.

AUTHOR CONTRIBUTIONS

Johanna Pilicita Carua - Conducted the experiments, characterized the samples and wrote the article. Sarah Briceño - Designed the experiments, characterized, analyzed the samples, and wrote the article. Gottfried Suppan - Designed the electrochemical characterization and analysis of the samples. Karla Vizuete and Alexis Debut - Measured the samples using the Transmission electron microscopy technique.

CONFLICTS OF INTEREST

There are no conflicts to declare.

REFERENCES

[1] Benalcázar, J., Lasso, E. D., Ibarra-Barreno, C. M., Arcos Pareja, J. A., Vispo, N. S., Chacón-Torres, J. C., and Briceño, S. (2022). Photochemical

Optimization of a Silver Nanoprism/Graphene Oxide Nanocomposite's Antibacterial Properties. *ACS omega*.

[2] Goncalves, G., Marques, P. A., Granadeiro, C. M., Nogueira, H. I., Singh, M. K., & Gracio, J. (2009). Surface modification of graphene nanosheets with gold nanoparticles: the role of oxygen moieties at graphene surface on gold nucleation and growth. *Chemistry of Materials*, 21(20), 4796-4802.

[3] Wei, H., Li, A., Kong, D., Li, Z., Cui, D., Li, T., ... & Guo, Z. (2021). Polypyrrole/reduced graphene aerogel film for wearable piezoresisitic sensors with high sensing performances. *Advanced Composites and Hybrid Materials*, *4*, 86-95.

[4] Lu, X., Qi, H., Zhang, X., Xue, Z., Jin, J., Zhou, X., & Liu, X. (2011). Highly dispersive Ag nanoparticles on functionalized graphene for an excellent electrochemical sensor of nitroaromatic compounds. *Chemical Communications*, *47*(46), 12494-12496.

[5] Lu, W., Luo, Y., Chang, G., & Sun, X. (2011). Synthesis of functional SiO2-coated graphene oxide nanosheets decorated with Ag nanoparticles for H2O2 and glucose detection. *Biosensors and Bioelectronics*, *26*(12), 4791-4797.

[6] Noor, A. A. M., Shahid, M. M., Rameshkumar, P., & Huang, N. M. (2016). A glassy carbon electrode modified with graphene oxide and silver nanoparticles for amperometric determination of hydrogen peroxide. *Microchimica Acta*, *183*, 911-916.

[7] Zhong, L., Gan, S., Fu, X., Li, F., Han, D., Guo, L., & Niu, L. (2013). Electrochemically controlled growth of silver nanocrystals on graphene thin film and applications for efficient nonenzymatic H2O2 biosensor. *Electrochimica Acta*, *89*, 222-228.

[8] Yang, Z., Qi, C., Zheng, X., & Zheng, J. (2015). Facile synthesis of silver nanoparticle-decorated graphene oxide nanocomposites and their application for electrochemical sensing. *New Journal of Chemistry*, *39*(12), 9358-9362.

[9] Saade, J., & de Araújo, C. B. (2014). Synthesis of silver nanoprisms: a photochemical approach using light emission diodes. *Materials Chemistry and Physics*, *148*(3), 1184-1193.

[10] Zhang, Q., Li, N., Goebl, J., Lu, Z., & Yin, Y. (2011). A systematic study of the synthesis of silver nanoplates: is citrate a "magic" reagent?. *Journal of the American Chemical Society*, *133*(46), 18931-18939.

[11] Çiplak, Z., Yildiz, N., & Çalimli, A. (2015). Investigation of graphene/Ag nanocomposites synthesis parameters for two different synthesis methods. *Fullerenes, Nanotubes and Carbon Nanostructures*, *23*(4), 361-370.

[12] Cobos, M., De-La-Pinta, I., Quindós, G., Fernández, M. J., & Fernández, M. D. (2020). Graphene oxide–silver nanoparticle nanohybrids: Synthesis, characterization, and antimicrobial properties. *Nanomaterials*, *10*(2), 376.

[13] Chook, S.W. and Chia, C.H. and Zakaria, S. and Ayob, M.K. and Chee, K.L. and Huang, N.M. and Neoh, H.M. and Lim, H.N. and Jamal, R. and Rahman, R.M.R.A. (2012) Antibacterial performance of Ag Nanoparticles and AgGO nanocomposites prepared via rapid microwave-assisted synthesis method. *Nanoscale Research Letters*, 7 (1). 541.

[14] Bae, Y., Kim, N. H., Kim, M., Lee, K. Y., & Han, S. W. (2008). Anisotropic assembly of Ag nanoprisms. *Journal of the American Chemical Society*, *130*(16), 5432-5433.

[15] Arcos-Pareja, J., Lasso, E. D., Ibarra-Barreno, C. M., Benalcázar, J., Robalino, K., Debut, A., Briceño, S., & Chacón- Torres, J. (2021). Revealing the Synthesis of Triangular Silver Nanoplates: A Study of the Photochemical Growth Mechanism around the pH

and Trisodium Citrate Variations. *physica status solidi (b)*, *258*(12), 2100189.

[16] Sharma, N., Sharma, V., Jain, Y., Kumari, M., Gupta, R., Sharma, S. K., & Sachdev, K. (2017). Synthesis and characterization of graphene oxide (GO) and reduced graphene oxide (rGO) for gas sensing application. In *Macromolecular Symposia* 376(1), 1700006.

[17] Suppan, G., Briones-Macías, M., Pazmiño-Arias, E., & Zamora-Ledezma, C. (2021). Fabrication and Characterization of Metal- Free Composite Electrodes Based on Few- Layer- Graphene Nanoplatelets for Oxygen Reduction Reaction Applications. *physica status solidi (b)*, *258*(5), 2000515.

[18] Gurunathan, S., Han, J. W., Park, J. H., Kim, E., Choi, Y. J., Kwon, D. N., & Kim, J. H. (2015). Reduced graphene oxide–silver nanoparticle nanocomposite: a potential anticancer nanotherapy. *International journal of nanomedicine*, *10*, 6257.

[19] Govindaraju, S., Ramasamy, M., Baskaran, R., Ahn, S. J., & Yun, K. (2015). Ultraviolet light and laser irradiation enhances the antibacterial activity of glucosamine-functionalized gold nanoparticles. *International journal of nanomedicine*, *10*(1), 67-78.

[20] Bansal, V., Li, V., O'Mullane, A. P., & Bhargava, S. K. (2010). Shape dependent electrocatalytic behaviour of silver nanoparticles. *CrystEngComm*, *12*(12), 4280-4286.

[21] Fayemi, O. E., Adekunle, A. S., & Ebenso, E. E. (2017). Electrochemical determination of serotonin in urine samples based on metal oxide nanoparticles/MWCNT on modified glassy carbon electrode. *Sensing and Bio-Sensing Research*, *13*, 17-27.

[22] Yuan, M. M., Zou, J., Huang, Z. N., Peng, D. M., & Yu, J. G. (2020). PtNPs-GNPs-MWCNTs-β-CD nanocomposite modified glassy carbon electrode for

sensitive electrochemical detection of folic acid. *Analytical and bioanalytical chemistry*, *412*, 2551-2564.

[23] Zoski, C. G. (Ed.). (2006). *Handbook of electrochemistry*. Elsevier.

[24] Kadara, R. O., Jenkinson, N., & Banks, C. E. (2009). Characterisation of commercially available electrochemical sensing platforms. *Sensors and Actuators B: Chemical*, *138*(2), 556-562.

[25] Lavagnini, I., Antiochia, R., & Magno, F. (2004). An extended method for the practical evaluation of the standard rate constant from cyclic voltammetric data. *Electroanalysis: An International Journal Devoted to Fundamental and Practical Aspects of Electroanalysis*, *16*(6), 505-506.

[26] Elgrishi, N., Rountree, K. J., McCarthy, B. D., Rountree, E. S., Eisenhart, T. T., & Dempsey, J. L. (2018). A practical beginner's guide to cyclic voltammetry. *Journal of chemical education*, *95*(2), 197-206.

[27] Zoski, C. G. (Ed.). (2006). *Handbook of electrochemistry*. Elsevier.

[28] Lu, X., Qi, H., Zhang, X., Xue, Z., Jin, J., Zhou, X., & Liu, X. (2011). Highly dispersive Ag nanoparticles on functionalized graphene for an excellent electrochemical sensor of nitroaromatic compounds. *Chemical Communications*, *47*(46), 12494-12496.

[29] Loock, H. P., & Wentzell, P. D. (2012). Detection limits of chemical sensors: Applications and misapplications. *Sensors and Actuators B: Chemical*, *173*, 157-163.

[30] Viswanathan, P., & Ramaraj, R. (2016). Polyelectrolyte assisted synthesis and enhanced catalysis of silver nanoparticles: Electrocatalytic reduction of hydrogen peroxide and catalytic reduction of 4-nitroaniline. *Journal of Molecular Catalysis A: Chemical*, *424*, 128-134.

[31] Peretyazhko, T. S., Zhang, Q., & Colvin, V. L. (2014). Size-controlled dissolution of silver nanoparticles at neutral and acidic pH conditions: kinetics and size changes. *Environmental science & technology*, *48*(20), 11954-11961.